Research article

Geoenergy

https://doi.org/10.1144/geoenergy2023-053 | Vol. 2 | 2024 | geoenergy2023-053

Fracture smectites in bedrock at the Kivetty and Romuvaara sites, Finland, as natural analogues for radioactive waste repository buffers

H. M. Reijonen[1]*, T. Al-Ani[1], T. Elminen[1], J. Kuva[1], K. Issukka[1] and R. Lamminmäki[2]

[1] Geological Survey of Finland (GTK), Vuorimiehentie 5, Espoo 02151, Finland
[2] Posiva Oy, Olkiluoto, Eurajoki 27160, Finland
HMR, 0000-0002-6665-4977; TA-A, 0000-0002-7586-6349; JK, 0000-0003-0241-6838; RL, 0000-0002-1620-1646
*Correspondence: heini.reijonen@gtk.fi

Abstract: Bentonite is used in various geological repository designs for highly radioactive and low- and intermediate-level waste. Stability of such materials has been evaluated in long-term safety assessments, with recent emphasis on potential chemical erosion of these clays in fresh groundwater conditions. The fracture-filling mineralogy at two investigation sites, Kivetty and Romuvaara, in Finland shows the existence of different types of smectites characterized by their respective dominant elements, such as Mg-, Fe- and Na–Ca-rich smectites. Of these, Ca- and Na-smectites are likely to be montmorillonites that provide potential natural analogues for the bentonite buffers and their long-term performance in fractured bedrock environments. The smectite minerals observed reflect the local parent rock mineral composition, suggesting *in situ* formation during hydrothermal alteration, well predating the current freshwater conditions in the fractured bedrock. These observations support the stability of smectites, including Na- and Ca-montmorillonites, in the fractured bedrock of glaciated terrain with fresh continental groundwater extending to repository-relevant depths. Further, no erosion or sedimentation processes have been observed to have taken place in the fracture systems studied. However, uncertainties remain related to detailed exchangeable cation compositions of the smectite. Current groundwater systems at both sites would alter the composition of montmorillonite towards the Ca-rich form, and more detailed investigations are required to assess the stability of Na-montmorillonite in connection to open fractures. In general, bentonite alteration in fractures to Ca-montmorillonite would be beneficial in repository scenarios that consider potential chemical erosion by dilute groundwater.

Supplementary material: Supplementary material 1 (XCT data for fracture smectite samples from Kivetty and Romuvaara) are available at https://doi.org/10.23729/1ce75faa-d52a-43cd-af40-3961b3081f70 [last accessed 5 July 2023] and Supplementary material 2 (XRD diffractogram data) and Supplementary material 3 (SEM-EDS data) are available at https://doi.org/10.6084/m9.figshare.c.7126477

Thematic collection: This article is part of the Sustainable geological disposal and containment of radioactive waste collection available at: https://www.lyellcollection.org/topic/collections/radioactive

Received 15 December 2023; **revised** 22 February 2024; **accepted** 7 March 2024

Bentonite is used as a buffer and backfill material in repository designs for geological disposal of spent nuclear fuel (e.g. SKB 2011; RWM 2017; Nagra 2021; Posiva 2021*a*) (Fig. 1a, b) and in some designs for low- and intermediate-level waste (e.g. Pusch 2003). Montmorillonite, the predominant mineral in most bentonites (e.g. Meunier 2005), is found in the Finnish bedrock, along with other smectites, as an alteration mineral from a range of geological processes (e.g. Uusinoka and Alkio 1976; Marcos 1989; Gehör *et al.* 1997*a*, *b*; Kärki *et al.* 1997; Front *et al.* 1998; Vartiainen 2005; Gehör 2007; Viola *et al.* 2011, 2013; Posiva 2021*b*; Nordbäck *et al.* 2023), providing potential analogues for buffer materials.

In Finland, the bentonite surrounding the waste container (see Fig. 1b) is planned to be of Na-type when installed in the deposition hole (Posiva 2021*c*) with *c*. 87 wt% of montmorillonite (e.g. Kiviranta *et al.* 2017) plus illite, muscovite, quartz, feldspars, carbonates, pyrite and gypsum. The exchangeable cation composition (ECC) of the reference bentonite is dominated by Na: e.g. 74% Na, 18% Ca, 7% Mg and 1% K (Kiviranta *et al.* 2017). However, groundwater–bentonite interaction will alter the ECC in the repository over time (see e.g. Posiva 2021*d*).

Chemical erosion, a process that may lead to the loss of swelling clay from repository components under low ionic strength conditions, may occur when sufficiently dilute groundwater comes into contact with bentonite in bedrock with advective pathways (fractures). In general, the processes of erosion and sedimentation within the bedrock fractures are taken into account in the safety cases that assess the performance of the geological repositories (e.g. Hjerpe *et al.* 2021). The erosion threshold or clay dispersion process depends on the ionic strength and composition of the groundwater, the initial composition of the clay, and the groundwater-flow conditions (e.g. Posiva 2021*d*). Generally, Na-bentonites are more prone to chemical erosion than Ca-bentonites (e.g. Birgersson *et al.* 2008; Kaufhold and Dohrmann 2008; Hedström *et al.* 2023). The total charge equivalent of cations in groundwater should remain above 8 mM to prevent chemical erosion, based on the cautious assumption that these cations are predominantly Na^+ (Posiva 2021*a*). Extensive experimental (e.g. Baik *et al.* 2007; Birgersson *et al.* 2008; Vilks and Miller 2010; Schatz *et al.* 2013, 2016; Svoboda 2013; Reid *et al.* 2015; Hedström *et al.* 2016; Börgesson *et al.* 2018; Alonso *et al.* 2018, 2019) and modelling (Liu *et al.* 2009; Neretnieks *et al.* 2009; Neretnieks *et al.* 2017; Börgesson *et al.* 2018) work has been carried out to assess the potential risk of the chemical erosion processes on the waste repositories (for a summary see Posiva 2021*d*); however, uncertainties still remain, some of them specific to the high water/

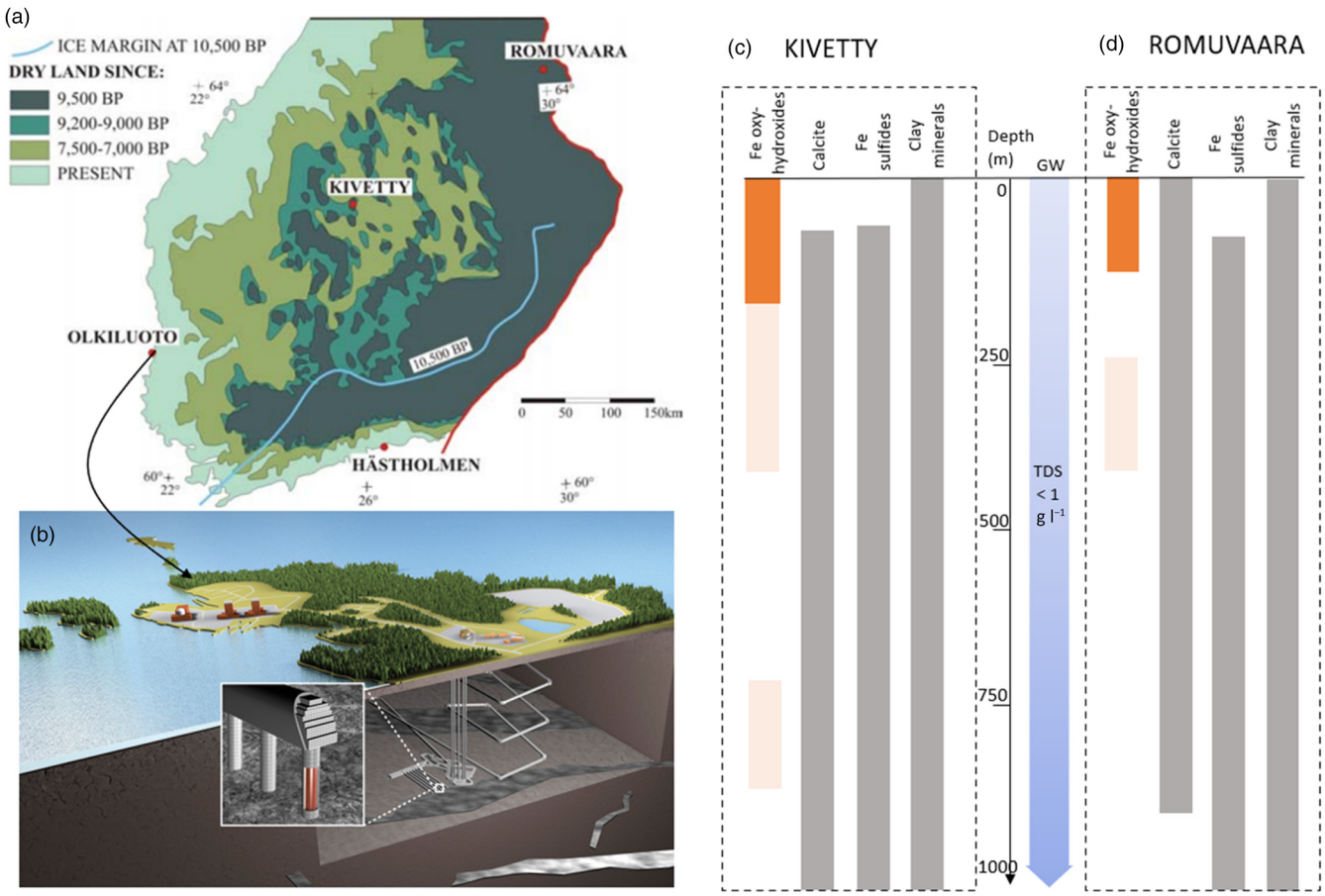

Fig. 1. (**a**) A map of post-glacial land uplift in Finland showing the studied sites at Kivetty and Romuvaara, and (**b**) Olkiluoto, where a geological repository is planned that will be utilizing bentonite-based materials to fill cavities in excavated spaces in crystalline bedrock. (**c**) and (**d**) The main fracture mineral groups occurring in currently fresh groundwater conditions (GW) for Kivetty and Romuvaara, respectively. Darker orange indicates a higher abundance than in the pale coloured area. Solid grey indicates common occurrence. BP, before present; GW, groundwater interval.
Source: (a) modified after Eronen *et al.* (1995); and (b) image courtesy of Posiva Oy.

rock ratios (e.g. Muurinen and Lehikoinen 1999) that may be encountered in bedrock fractures surrounding the bentonite in the repositories. Observations from field conditions (Posiva 2021*b*) do not support the likelihood of erosion of the bentonite buffer (Posiva 2021*c*, *e*).

Given the concern (e.g. Posiva 2021*d*) about potential bentonite loss under dilute groundwater conditions, the stability of the natural smectites at the Kivetty and Romuvaara sites in Finland (Fig. 1) are examined here as potential natural analogues (see Reijonen *et al.* 2023 for a definition of, and a discussion of the uses of, natural analogues) for the long-term performance of engineered bentonite barriers in a repository. The presence of smectite (especially montmorillonite) in bedrock fractures at these sites (e.g. Gehör *et al.* 1997*a*; Kärki *et al.* 1997) is a powerful argument for the longevity of bentonite stability under similar conditions, while detailed data for repository safety cases are currently lacking (e.g. Reijonen and Alexander 2015; Reijonen and Marcos 2016). The main objective of this study is to assess the mode of occurrence and mineralogy of the natural smectites in such localities.

Geological context

The formation of fracture-filling minerals is dependent on the composition of the parent rocks and the overall hydrogeochemical conditions. For open water–rock systems in granitic environments, clay minerals are formed at shallow depths as products of feldspar weathering. Kaolinite is formed in environments where alkali and alkaline earth metals are readily leached out of the system. In water–feldspar systems with a low groundwater flow rate, from which the alkali and alkaline earth metals cannot be readily removed, the resulting high potassium level actively promotes the illitization of feldspars (Alekseyev *et al.* 1997; Zhu and Lu 2009). With the accumulation of calcium (or magnesium or sodium) in the system, swelling clays such as montmorillonite can be formed. In addition to weathering, hydrothermal alteration produces smectites at low temperatures (<160°C) through hydrolysis reactions of silicate phases (plagioclase, feldspar, pyroxene, olivine, volcanic glass, biotite and micas) (e.g. see Aaltonen *et al.* 2018; Fulignati 2020). An example of such a reaction is (equation 1):

$$1.17NaAlSi_3O_8 + H^+ = \underset{\text{Albite}}{} \; 0.5Na_{0.33}Al_{2.33}Si_{3.67}O_{10}(OH)_2 + 1.67SiO_2 + Na^+ \quad (1)$$
Na-montmorillonite

Long-term repository safety assessments commonly discuss future scenarios for up to 1 Myr (e.g. NEA 2012; ASC 2023), during which changes will be induced in the bedrock due to climatic- and denudation-related processes. Geochemical reactions can occur during infiltration of meteoric (or glacial melt) waters into fractured bedrock systems. Dilution of the groundwater can occur via two pathways, either by prolonged infiltration of meteoric water during temperate climatic conditions or during infiltration of glacial meltwater during glacial conditions (melting phases). Dilution effects on the groundwater chemistry in the fractured rock depend on the configuration of the hydraulic structures and properties onsite, regional topography, overburden and the initial groundwater composition. In the case of glacial or periglacial conditions,

additional pressure induced by ice and permafrost conditions will also affect the degree of infiltration (e.g. Claesson Liljedahl *et al.* 2016). Any infiltrating water will then mix with the existing groundwater in the rock (e.g. see SKB 2019; Posiva 2022).

Both research sites (Fig. 1) selected for this study record the present-day dilute conditions at repository-relevant depths (Pitkänen *et al.* 1998; Anttila *et al.* 1999*b*). The Kivetty site lies in the Svecofennian granitoid complex of central Finland (with an age of *c*. 1880 Ma). The bedrock at Kivetty consists mostly of porphyritic or equigranular granodiorite–granite with minor occurrences of gabbro (Anttila *et al.* 1992). These have been metamorphosed and deformed in two phases, and brittle deformation features are common but decrease with depth. Based on previous studies (Lindberg and Paananen 1989, 1990, 1992; Gehör *et al.* 1995, 1996*a*, 1997*a*, 1998), the most common fracture minerals at Kivetty are calcite, iron sulfides and iron oxyhydroxides (Fig. 1c). Clay minerals, iron oxides and quartz occur in lesser quantities. The bedrock at Romuvaara (2800 Ma) is in the Archean basement complex of eastern Finland. Typical rock types are migmatitic banded gneisses (tonalite, leucotonalite and mica gneiss) that are cross-cut by granodiorite and metadiabase dykes (Anttila *et al.* 1999*b*). The reported fracture mineral studies have focused on existing/geologically recent water-conducting fractures (Gehör *et al.* 1996), and the most common fracture minerals are calcite, iron sulfides, iron oxyhydroxides and clays (Fig. 1d). At both sites some uncertainty exists in the knowledge of paragenetic relationships, and minerals observed in the same assemblage are not necessarily formed synchronously (Gehör *et al.* 1995, 1996*a*, *b*).

The hydrogeochemical evolution at both sites is well known (Pitkänen *et al.* 1998; Anttila *et al.* 1999*b*). Salinity and the degree of water–rock interaction are low. The low salinity is typical for an old crystalline bedrock environment that has experienced episodes of meteoric water infiltration (including glacial melting) over an extended period during the Quaternary. Based on thermodynamic stability calculations by Pitkänen *et al.* (1996, 1998), the groundwaters at the study sites in general would favour the alteration of the bentonite buffer mass (assuming an original Na-form) towards Ca-, Mg- and K-smectite but at a negligible level, based on the consideration of buffering capacity in the large mass of buffer filling the repository cavities (Melamed *et al.* 1992; Muurinen *et al.* 1996; Pitkänen *et al.* 1996, 1998). However, the solid/liquid ratio can be much smaller in bedrock fractures than in the bentonite buffer, potentially leading to a different and ranging exchangeable cation composition (ECC) of montmorillonite at lower densities (cf. Muurinen and Lehikoinen 1999) than calculated for compacted bentonite buffers. At both sites, while smectite is observed at all depths (down to *c*. 1 km), calcite is almost absent from the topmost parts of the bedrock (Fig. 1c, d) due to dissolution by meteoric water close to the bedrock surface (Pitkänen *et al.* 1996, 1998). This would suggest a higher relative stability of smectite over calcite, even in conditions of relatively recent meteoric water infiltration.

The fracture clays are likely to represent very old alteration phenomena (e.g. Hall *et al.* 2021; Nordbäck *et al.* 2023). The most recent geological event potentially increasing the temperature of the bedrock was related to burial under sedimentary cover, which thinned out towards the east, during the Paleozoic: that is, at least 250 Ma (e.g. see Larson *et al.* 1999). However, the ages reported from apatite fission-track dating for Kivetty and Romuvaara show even older ages for low-temperature conditions: *c*. 605–290 and *c*. 900–543 Ma, respectively (Larson *et al.* 1999). Even older ages are known for fault gouge illites from south to southern Finland, which range from 967.6 ± 19.7 to 697.3 ± 14.1 Ma from Myras (Elminen *et al.* 2018) and from 1549.7 ± 31.7 to 561 ± 11.2 Ma from Olkiluoto (Mänttäri *et al.* 2007; Viola *et al.* 2011, 2013; Nordbäck *et al.* 2023). Many of the samples from Olkiluoto (Viola *et al.* 2011, 2013; Nordbäck *et al.* 2023) contain smectites, smectite–illite or smectite–vermiculite, constrained not just for illitization but also indicating likely significantly older (>250 Ma) ages for the formation of smectites (hypothesized to be retrograde and likely to have been formed subsequent to illite at lower temperatures). Thus, smectite formations can be considered to be at least 250 Ma, especially at depth where weathering phenomena can be ruled out.

In this study we record the mineral composition of factures in granitoid rocks of Finnish bedrock, and attempt to document the geological processes that reflect the existence and long-term stability of clay minerals in conditions that correspond to those in the buffer and backfill material of repository designs.

Materials and methods

Two boreholes from Kivetty (KI-KR1 and KI-KR5) and one borehole from Romuvaara (RO-KR2) were sampled for fracture-filling clays ($n = 35$). An analysis of the <63 μm clay fraction was carried out using X-ray diffraction (XRD) and scanning electron microscopy (SEM). Thin sections and fracture surface samples were prepared for microscopy and SEM-EDS (energy dispersive X-ray spectroscopy) examination. The samples and analytical techniques are listed in Table 1.

X-ray computed tomography

X-ray computed tomography (XCT) was carried out with a GE Phoenix V|tome|x S, using a 240 kV microfocus tube and with 0.5 mm of Cu used as a beam filter. At each angle the detector waited for a single exposure time and then took an average over three exposures. Some samples were scanned as vertical multiscans, where several scans were combined into a single 3D image. Samples for the XCT were selected based on several chosen fracture types of interest in hand specimens in order to obtain information on the fracture-filling material inside the drill core.

XRD

From the sheared and fractured surfaces of the Kivetty KR1 and KR5 and the Romuvaara KR2 drill core samples, powder of the secondary alteration minerals was extracted manually under a binocular microscope. The aim was to collect as much homogeneous clay material from each fracture as possible whilst trying to avoid sampling the underlying igneous or metamorphic silicates and the possibly earlier crystallized carbonate or chlorite layers underlying the clay filling.

For X-ray powder diffraction (XRPD) measurements, part or all the fracture material was ground manually in an agate mortar in an acetone suspension, poured onto a glass slide, spread evenly and then dried. Samples were measured using a Bruker D8 Discover Bragg-Brentano powder diffractometer equipped with a Cu tube, 0.3° fixed divergence slit, 2.5° sollers, beam knife, spinner, Ni filter and Lynxeye silicon strip detector. Powder diffractograms were measured from the 4°–71.5° 2θ range using 40 kV and 40 mA power settings in continuous mode, 0.02° 2θ s^{-1} for 1 h/sample. Relative humidity was measured during the analysis and varied between 30 and 40%. Phase identifications were carried out using Bruker EVA software and the International Centre for Diffraction Data (ICDD) PDF-4 (Powder Diffraction File) Minerals 2020 database. The presence of smectite-group clay was tested by wetting the sample with a few drops of ethylene glycol (EG), stored in a EG desiccator overnight, and then analysing using the same settings as above. For samples with very small amounts of powder, the excess EG layer resulted in a high amorphous background noise level. Nonetheless, in the low 2θ range, clear peaks were detected.

Table 1. Samples and analytical plan

Drill hole	Depth from* (m)	Depth to* (m)	Type	XCT	XRD	SEM-EDS drill core	SEM-EDS thin section
KI-KR1	46.20	46.25	o		x		
KI-KR1	56.71	56.98	o	X	x	x	x
KI-KR1	262.78	262.90	o		x		
KI-KR1	326.90	327.00	o		x		
KI-KR1	398.10	398.20	o		x		
KI-KR1	398.58	398.74	o	X	x	x	
KI-KR1	399.30	399.45	o		x		
KI-KR1	403.06	403.10	o		x		
KI-KR1	504.84	504.92	o		x		
KI-KR1	536.93	537.04	o		x		
KI-KR1	537.18	537.23	o		x		
KI-KR1	539.30	539.35	o		x		
KI-KR1	544.40	544.48	o		x		
KI-KR1	561.95	562.05	o		x	x	
KI-KR1	650.70	650.80	c	X	x	x	
KI-KR5	669.41	669.47	o/c		x	x	
KI-KR5	720.76	720.92	c		x		
KI-KR5	741.98	742.02	o/c		x		
KI-KR5	756.90	756.97	c		x		
KI-KR5	766.69	766.82	o		x		
KI-KR5	781.46	781.58	c		x		
KI-KR5	781.73	781.83†	c	X	x		
KI-KR5	781.83	782.12†	c	X		x	x
RO-KR2	203.70	203.80	c	X	x	x	x
RO-KR2	218.25	218.29	o		x		
RO-KR2	226.90	227.00	o		x		
RO-KR2	306.77	306.82	o		x	x	
RO-KR2	341.30	341.33	o		x		
RO-KR2	397.12	397.22	o		x	x	
RO-KR2	422.47	422.54	o		x		
RO-KR2	441.57	441.62	o		x	x	
RO-KR2	574.92	575.05	o		x	x	
RO-KR2	831.35	831.47	o		x		
RO-KR2	834.56	834.66	o/c		x		
RO-KR2	882.35	882.40	o		x	x	

*Depth along the drill hole (KI-KR1 and RO-KR2 dip 75°l Ki-KR5 dip 68°); †samples from the same long fracture.
Type, fracture type assessed during sampling (o, open; c, closed; o/c, not clear).
XCT, X-ray computed tomography; XRD, X-ray diffraction; SEM-EDS, scanning electron microscopy + energy dispersive X-ray analysis.

Petrography

Three polished thin sections (30 μm thick) of selected samples with an abundance of fracture-filling minerals (KI-KR1_56.71m, KI-KR5_781.83m and RO-KR2_203.70m) were prepared at the Thin Section Lab, Toul, France. The thin sections were made using oil instead of water during grinding and polishing to preserve the swelling clays in the samples. The thin sections were studied for petrology and mineralogy using polarized light and scanning electron microscopes.

SEM-EDS

Detailed studies of both the thin sections and the fracture-filling surface samples were carried out by SEM-EDS analyses. The drill-core samples consisted of half-cores that were *c*. 4 cm in diameter and 20–25 cm in length (Fig. 2). These samples were selected based on the XCT and XRD results in order to obtain data from fractures of interest with different mineralogical properties. Backscattered electron (BSE) images and the chemical compositions of fracture-filling minerals were collected using an Hitachi SU3900 SEM equipped with an Oxford Instruments EDS-spectrometer X-Max 20 mm^2 (SDD). BSE images were used to document smectite and other clay minerals at ×100 and ×5000 magnifications. EDS was used in the semi-quantitative chemical analysis for the identification of each mineral phase using a 20 kV accelerating voltage and 1 nA probe current.

Results

XCT

The XCT 3D imaging confirmed the different fracture types defined during the sampling and guided the thin section location selection to examine open, closed and multiphase fracture-filling materials (see Supplementary material 1). Sample KI-KR1_56.71m showed an open fracture, seen as black in the greyscale image (Fig. 3a), with fine-grained fracture-filling material. Sample KI-KR5_781.83m was confirmed to contain a closed fracture type (Fig. 3b). Sample RO-KR2_203.70m has been assigned as closed based on drill core logging; XCT imaging additionally shows a layered structure in the filling material, suggesting multiple phases of fracture mineral growth (Fig. 3c).

Optical petrography

The petrographical thin sections of the granitic rocks (KI-KR1_56.71 and KI-KR5_781.83m) from Kivetty contain the mineral assemblage plagioclase, quartz, biotite, Fe–Ti oxides, hornblende and K-feldspar (Fig. 4a–d). The sample (RO-KR2_203.70m) from the Romuvaara

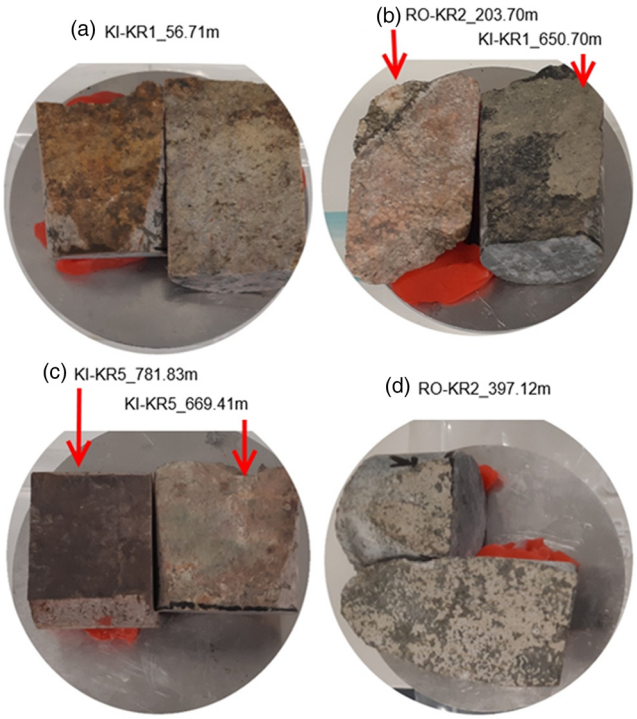

Fig. 2. Photographs of drill-core samples showing representative fracture surface/vein fillings and associated clay minerals.

area has a similar mineral composition but lacks hornblende (Fig. 4e, f). Fracture-filling minerals at Kivetty are mainly clay minerals, carbonates (calcite), chlorites, iron sulfides and epidote (Fig. 4a–d). The alteration of mafic minerals such as biotite and hornblende to chlorite (Fig. 4b) and the replacement of plagioclase by calcite and sericite (Fig. 4c, d) can be clearly seen. The sample from Romuvaara (Fig. 4e, f) shows the textural relationship between the secondary mineral formations (clay appearing secondary to carbonate formation). Fragments of the main rock-forming minerals are also seen in the fracture-filling assemblages. There is no significant difference between the origins of the fracture-filling clay for the two sites, both show typical products of hydrolysis reactions and hydrothermal alteration (cf. Weisenberger and Bucher 2011).

XRD

The XRD phase identification results from the fracture minerals are provided in Table 2. The sampling was focused on the fracture-filling material but the adjacent wall components were also usually present in the preparation due to the inclusion of very small amounts of host-rock phases in the fracture-filling material (fracture widths were mostly <1 mm; see Fig. 2). The primary minerals observed in XRD included quartz, albite, microcline, biotite, muscovite and amphibole. Some of the analysed quartz, albite and micas can also occur as secondary occurrences in the fracture-filling material. The most common fracture minerals identified by XRD were calcite and clay minerals. Accessory minerals detected included REE fluorcarbonate (synchysite, a common hydrothermal accessory mineral), muscovite, phlogopite, annite, pyrophyllite and hematite.

The clay minerals detected included smectite group minerals, illite, chlorite and mixed-layer phases. Kaolinite/serpentine and talc were identified in some samples. Smectite group minerals were present in almost all samples. Smectite was identified from air-dried samples by its (001) peak at 14–15 Å d-spacing range but, in three samples, the main peak of montmorillonite was close to 12 Å, suggesting potentially Na as the main exchangeable cation (Brindley and Brown 1980). Smectite samples showed a shift of (001) reflection towards 17 Å after ethylene glycol (EG) treatment. Only five samples showed a peak shift to 16.5 Å or more; with most samples the expansion was smaller, to about 15 Å. This could indicate the presence of mixed-layer clays, where illite, chlorite or vermiculite layers are mixed with the smectite layers in the mineral structure. Diffractograms are provided in Supplementary material 2.

SEM-EDS from drill-core samples and polished TS

SEM-BSE imaging and SEM-EDS analyses were performed on cut drill-core samples and polished thin sections. By observing the clay mineral morphologies and their chemical compositions, it was possible to establish that smectite and chlorite were the dominant components in most of the analysed samples, with a minor amount of illite and kaolinite.

The SEM images of the surface fractures in cut drill cores (Fig. 5) and polished thin sections (Fig. 6) showed morphologies ranging from typical thin platy/flaky shapes to swirly features and honeycomb textures, which are characteristic of clay minerals with a smectitic (often authigenic) composition (cf. Fesharaki *et al.* 2007; Iacoviello *et al.* 2012). Kaolinite and illite occur as book-like forms and as platy or scalloped forms, respectively. Mixed-layer clays, intermediate products of clay mineral transition and alteration, are also present in some samples, such as smectite–chlorite (S/C), smectite–illite (S/I) and illite–chlorite (I/C). An overview on the minerals detected with SEM-EDS in the thin sections and drill-core samples is provided in Table 3, while the full

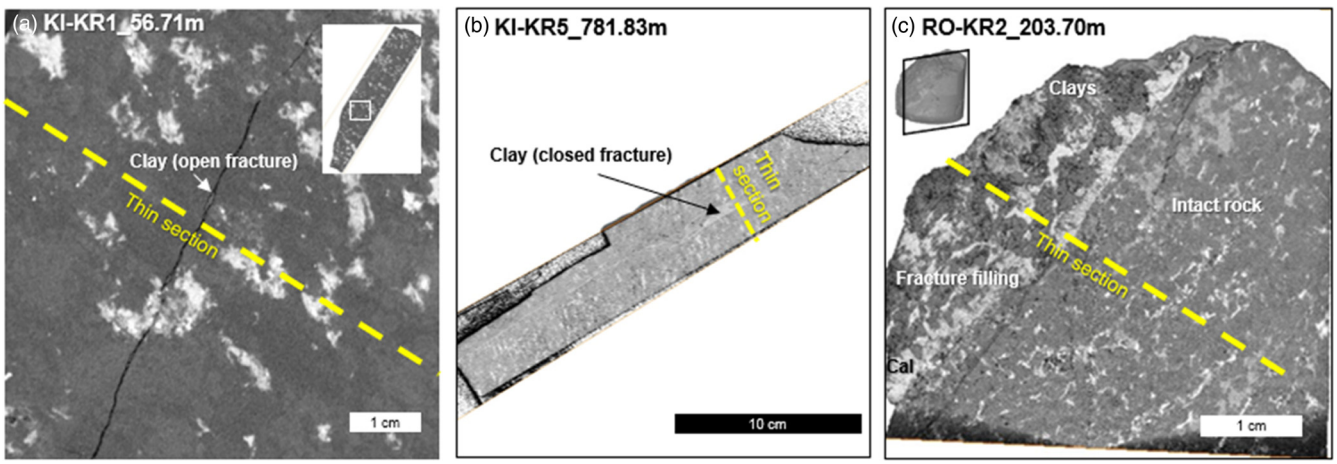

Fig. 3. (**a**–**c**) X-ray computed tomography (XCT) cross-section of the samples selected for thin section (locations are marked with dashed lines). The greyscale denotes the density differences in the sample.

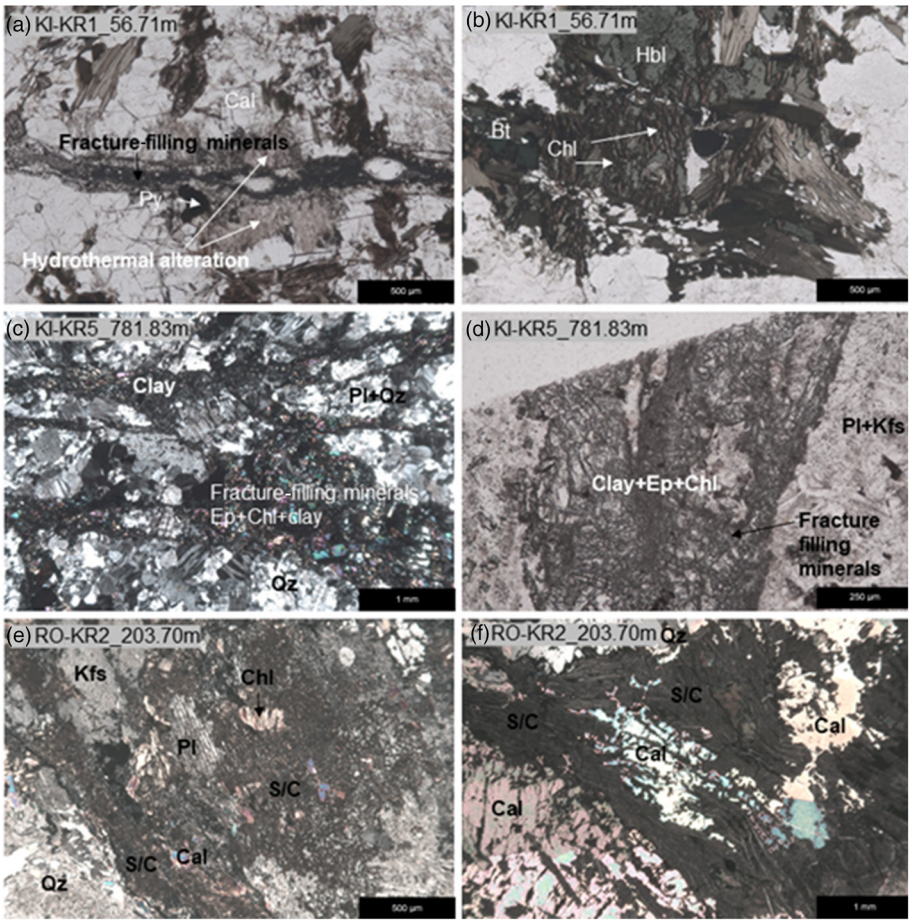

Fig. 4. Microphotographs (plain polarized light) of clay fracture filling and mineral alterations of sample KI-KR1_56.71m showing (**a**) fracture-filling minerals and (**b**) alteration of biotite and hornblende to chlorite; (**c**) and (**d**) sample KIKR5_781.83m showing the development of fracture-filling minerals; and (**e**) and (**f**) sample RO-KR2_203.70m of showing replacement of plagioclase by calcite and clay minerals. Appreviations: Cal, calcite; Py, pyrite; Bt, biotite; Hbl, hornblende; Chl, chlorite; Qz, quartz; Ep, epidote, Pl, plagioclase; Kfs, K-feldspar; S/C, smectite-chlorite.

dataset of SEM-EDS clay mineral compositions is given in Supplementary material 3.

In sample KI-KR1_56.71m the smectite particles occur as a cellular texture with dimensions ranging from 5 to 10 μm (Fig. 5a). This sample, taken close to the bedrock surface from an open fracture, may have been affected by some weathering reactions. Sample KI-KR1_398.58m shows that smectite aggregates occur as a cornflake or cellular texture associated with radiating platelets of clinochlore (Fig. 5b). A thin platy/flaky morphology of smectite is clearly observable in samples KI-KR1_398.58m and RO-KR2_441.57m (Fig. 5c, d). Samples from both sites have a minor occurrence of disseminated synchysite, confirming the XRD observations (not in the same samples, which is likely to be due to the very small sample amounts available for XRD). Synchysite occurs in the same fracture-filling mass as smectite, suggesting the simultaneous formation of synchysite with late-stage clays, sometimes replacing them (Fig. 5c, d). In addition, the BSE images of samples RO-KR2-306.77m and RO-KR2_203.70m show smectite composed of fine platy particles (1–5 μm) associated with S/I and S/C mixed-layer phases (Fig. 5e, f).

The analysis of clay mineral compositions using SEM-EDS is not an accurate technique. Potential problems in the SEM-EDS interpretation arise from the poor resolution, electronic beam penetration through very thin materials such as clay minerals, and incorrect measurement geometry of the rough mineral surface compared to a flat polished surface. The electron beam is powerful enough to penetrate through a thin mineral (clays) into any underlying mineral grain. This gives rise to the weak detection of elements from the studied mineral grain and the addition of elements from other surrounding mineral grains (cf. Welton 2003). Thus, the SEM-EDS data are treated semi-quantitatively in this study.

Different clay mineral phases, mainly composed of Si, Al, Fe, Mg, K, Ca and Na, were recognized based on the SEM-EDS analysis. The full dataset of SEM-EDS clay mineral compositions is presented in Supplementary material 3. EDS analyses of clay minerals with major elements of Si, Al, Fe, Mg, Ca and Na were interpreted as Ca- and Na-montmorillonites, whereas Si, Al, K and Fe were interpreted to be illitic in composition. SEM-EDS cannot determine whether the analysed Ca and Na are present in the smectite crystal structure or in the surrounding phases, obviously creating uncertainty in the results. However, by targeting the analyses on smectite textures (based on BSE images), it is possible to obtain at least indicative data on the potential smectite composition. In most of the studied samples, the EDS spectrum also indicates the presence of Mg in smectite that is associated with clinochlore (Mg-rich chlorite) to form mixed-layer S/C. Mixed layers of S/I were also identified in some samples, their elemental composition consisting of Si, Al, and minor amounts of K, Ca, Na, Mg and Fe.

SEM-EDS analysis results from the three thin sections confirm that the dominating fracture-filling clays are smectites occurring with chlorite, pyrite, Fe oxides and calcite. Clear indications of various types of argillic alteration can be observed. In the sample KI-KR1_56.71m, Na–Ca-smectite fracture filling in plagioclase (Pl) was observed (Fig. 6a). It had been formed in the open fracture planes, probably due to the release of lithostatic stress, accompanied by fluid penetration and subsequent alteration via plagioclase dissolution. The feldspar of the host rock in the vicinity of a fracture flow path can be easily dissolved by the attack of H^+ in flowing fluids (e.g. in hydrothermal waters). Na–Ca-smectite is often presumed to have formed by chemical weathering and dissolution–precipitation from feldspar in the presence of fluids allowing hydrolysis (Fig. 6a, b) (e.g. Kadir 2007). In Kivetty, Na–Ca-

Table 2. Qualitative XRD results divided as major, minor and trace phases in samples (smectite-bearing phases are shown in bold type)

Sample ID	XRD major	XRD minor	XRD trace	Hydraulic conductivity (K) ($m\ s^{-1}$) (interval measured given in parenthesis)	Groundwater sampling interval (m along the drill hole)
KI-KR1_46.20	Qz, Ab, Bt	Kfs	Cal		No sample
KI-KR1_56.71	**Sm (Na-Mt)**	Qz, Ilt	Kfs		No sample
KI-KR1_262.78	Cal, **Sm**, Chl	Mi, Qz	Cam, Ctl		No sample
KI-KR1_326.90	Qz, **Sm**	Ab, Kfs, Mi			300–345
KI-KR1_398.10	**Sm**, **Mxly**	Qz			370–415
KI-KR1_398.58	Qz, Cal, Chl	**Mxly**, Mc, Ab	Mi, Tlc	3.0×10^{-8} (395.5–399.5 m)	370–415
KI-KR1_399.30	**Sm (Na-Mt)**, Chl, Bt	Qz, Ab		3.0×10^{-8} (395.5–399.5 m)	370–415
KI-KR1_403.06	**Sm (Na-Mt)**		Mi, Cal, Qz		370–415
KI-KR1_504.84	**Sm**		Mi, Kfs		No sample
KI-KR1_536.93	**Sm**, Chl, **Mxly**, Bt	Cal, Cam			515–555
KI-KR1_537.18	Chl, Mi	Qz, Cal	Kfs		515–555
KI-KR1_539.30	Bt, Chl	Qz, Ab, Kfs, Cam, **Sm**		4.9×10^{-7} (537.7–539.7 m)	515–555
KI-KR1_544.40	**Sm**/Vrm, Ilt	Cam	Qz, Ab		515–555
KI-KR1_561.95	**Mxly**, **Sm**	Qz	Mi		No sample
KI-KR1_650.70	**Sm**, Ms, Chl	Cal, Qz, Kln	Ab, Mc, Cam		No sample
KI-KR5_669.41	Qz	**Sm**, Mi, Ab, Mc	Chl		No sample
KI-KR5_720.76	Qz, Ab, **Mxly**	Kfs, Ilt	Cal, Hem, Kln		No sample
KI-KR5_741.98	**Mxly** (S/C)	Qz	Chl	5.8×10^{-6} (740.4–742.4 m)	735–853
KI-KR5_756.97	Qz, Ab, Kfs, **Mxly**	Ilt	Prl		735–853
KI-KR5_766.69	Phl, Qz	Cam, Chl, Ab, Kfs			735–853
KI-KR5_781.46	Qz, Ep, **Mxly**	Ilt, Ab, Kfs	Chl, Kln		735–853
KI-KR5_781.73	**Sm**, Chl, Qz	Ab, Kfs, Mi	Syn (Ce), Hem, Cam		735–853
RO-KR2_203.70	**Mxly**, Cal	Qz	Ctl		No sample
RO-KR2_218.25	Ms		Chl, Ab		No sample
RO-KR2_226.90	Qz, Ab, Ms, Phl, Kfs, **Mxly**	Cal, Chl			No sample
RO-KR2_306.77	**Mxly** (S/C), **Sm**, Ms	Qz, Ab	Cal, Syn (Ce)		305–345
RO-KR2_341.30	Ms	**Mxly** (S/C), Ab	Qz, Kln, Cal	2.4×10^{-9} (340.3–346.5 m)	305–345
RO-KR2_397.12	Cal	**Sm**, Ms			375–415
RO-KR2_422.47	Ms, **Mxly**	Chl, Ab, Kfs		2.4×10^{-5} (415.0–422.2 m)*	No sample
RO-KR2_441.57	**Sm**, Chl, Phl	Ab, Cal			No sample
RO-KR2_574.92	**Sm**	Mi	Cal, Tlc	†	No sample
RO-KR2_831.35	Ms, **Sm**	Ab	Chl	†	No sample
RO-KR2_834.56	**Sm**, **Mxly**, Ms, Kfs	Ab, Chl	Syn	†	No sample
RO-KR2_882.35	Chl, Ms, Phl	Ab, Kfs	**Sm**, Qtz	†	No sample

Mineral abbreviations: Ab, albite; Cal, calcite; Cam, clinoamphibole; Chl, chlorite; ClC, clinochlore; Ctl, chrysotile; Hem, hematite; Ilt, illite; Kfs, K-feldspar; Kln, kaolinite; Mc, microcline; Mi, mica; Ms, muscovite; Mxly, mixed layers; Phl, phlogopite; Prl, pyrophyllite; Qz, quartz; S/C, smectite–chlorite; Sm, smectite; Syn, synchysite; Tlc, talc; Vrm, vermiculite. Potential Na-Mt (Na-montmorillonite) occurrences are indicated based on first low-angle reflection at 12 Å. Most smectites have 001 peak position around 14–15 Å (probably Ca-Mt (Ca-montmorillonite)) (Brindley and Brown 1980). Available hydraulic conductivities and groundwater sampling intervals are as indicated in Pitkänen *et al.* (1996, 1998).
*Conductive fractures reported down to 425.5 m (Pitkänen *et al.* 1996); †no measurements reported below 500 m (Pitkänen *et al.* 1996).

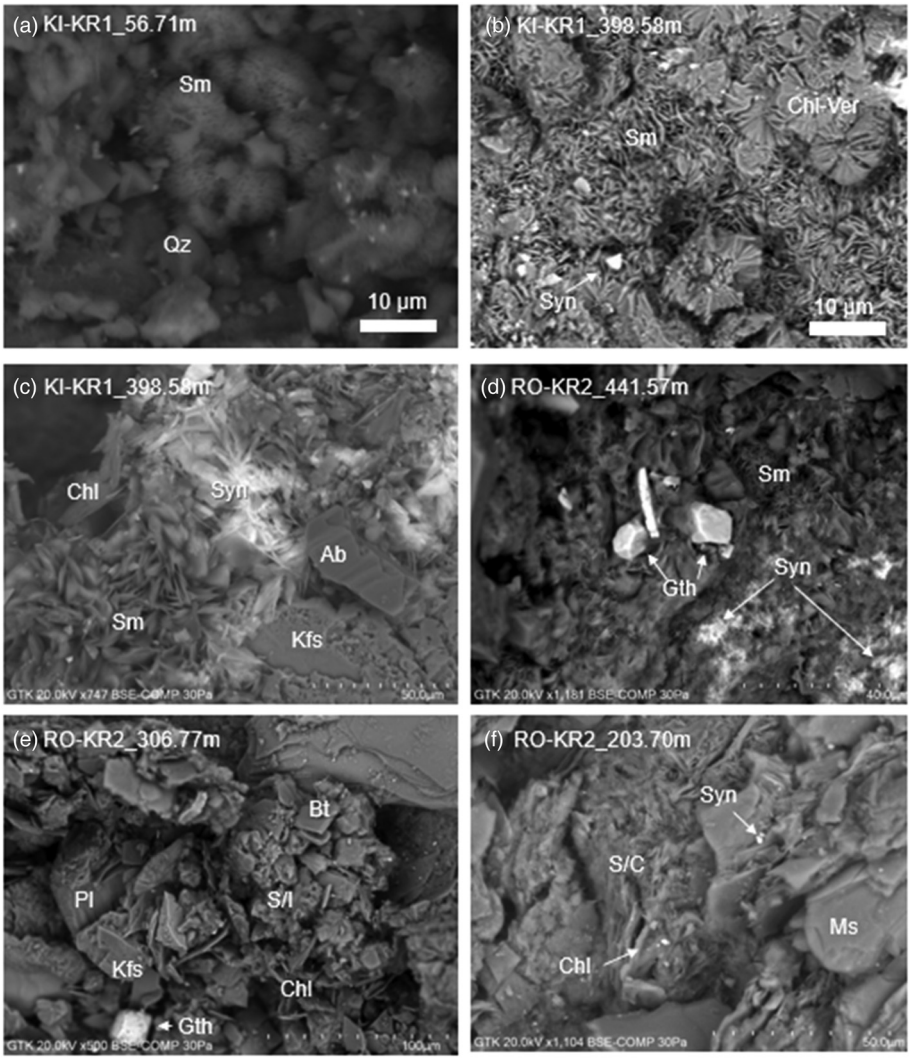

Fig. 5. SEM images of clay fracture filling in drill-core samples. (**a**) SEM image of the honeycomb morphology of smectite (Sm). (**b**) Smectite cornflake or cellular texture associated with radiating platelets of clinochlore in vermiform (Chl-Ver). (**c**) Thin platy/flake of smectite associated with REE carbonate (synchysite: Syn). (**d**) Smectite as curled leaves in contact with Syn and goethite (Gth). Platy fine particles of montmorillonite associated with (**e**) smectite–illite (S/I) and (**f**) smectite–chlorite (S/C) mixed layers. Additional abbreviations: Qz, quartz; Syn, synchysite; Chl, chlorite; Pl, plagioclase; Bt, biotite; Kfs, K-feldspar; Ms, muscovite.

smectite, interpreted as montmorillonite, occurs in sealed micro-fractures (Fig. 6a) as part of a larger open fracture in the sample (Table 1). In addition, Na–Ca-smectite is observed as precipitates within fractures along K-feldspar–plagioclase grain boundaries (Fig. 7a). In the same sample, smectites were observed as alteration minerals of plagioclase and hornblende (Fig. 6b). The sample also show partial chloritization of biotite and precipitation of Fe-smectite in microfractures and in the dissolution pores (Fig. 6c). Smectite was detected as a partial or total transformation product of hornblende, as shown in sample KI-KR5_781.83m, producing Mg-smectites on the centre of the grain and S/I in the rim of the hornblende and plagioclase grains (Fig. 6d).

SEM-EDS results of the RO-KR2_203.70m sample allow an interpretation of the textural relationship between the secondary carbonate and clay in the fracture network. Smectite, mixed-layer S/C and calcite are the main secondary mineral deposits sealing these fractures (Fig. 6e, f). Similar dissolution features as those for Kivetty are seen as Na–Ca-smectite clusters in pore-/fracture-filling material and replacing feldspars (Fig. 7b). The smectites occur due to hydrothermal alteration paragenesis, and are a typical product of hydrolysis reactions at the expense of microcline and plagioclase. Alkaline pH and low redox potential in the groundwater are factors that may favour the formation of smectite and calcite (Lima *et al.* 2011). Furthermore, XCT imaging of the sample RO-KR2_203.70m (Fig. 3c) shows that calcite has formed in association with smectite, producing a layered mass of denser (lighter grey in XCT image) calcite as coarse-grained fracture-filling and less dense (darker grey) smectite and S/C.

Based on the SEM-EDS analysis of thin sections, the clay phases result from intensive leaching of the primary minerals of the granitic host rocks by the infiltration of the hydrothermal fluids, as illustrated in Figures 6 and 7.

In understanding the uncertainties mentioned above regarding the semi-quantitative SEM-EDS data, clay analytical data from SEM-EDS were used to examine the overall chemical compositions (Fig. 8) to check the overall assessment of smectites present and to exhibit the overall similarity of duplicate samples analysed both from cut rock samples and thin sections. The chemical composition of most samples reflects advanced alteration and the presence of smectites (Fig. 8a). Large variations are seen in the overall percentiles of K, Na and Ca, highlighting the difficulty in assessing the smectite composition based solely on these chemical data and reinforcing the need for textural and petrographical support analysis (Fig. 8b).

Discussion

Hydrothermal alteration at both sites was mainly focused on the fractures with previously known alteration overprints of muscovite/sericite, carbonate and epidote, with the Romuvaara site exhibiting more extensive alteration than that found at Kivetty (e.g. Pitkänen *et al.* 1996). At the Kivetty site, there is clear evidence of altered, porous (e.g. Anttila *et al.* 1999*a*) hydrothermal zones from several drill holes (Gehör *et al.* 1995), including the drill hole KI-KR5 that is included in this study. However, our sampling was targeted on fractures located outside of this porous zone. At Kivetty,

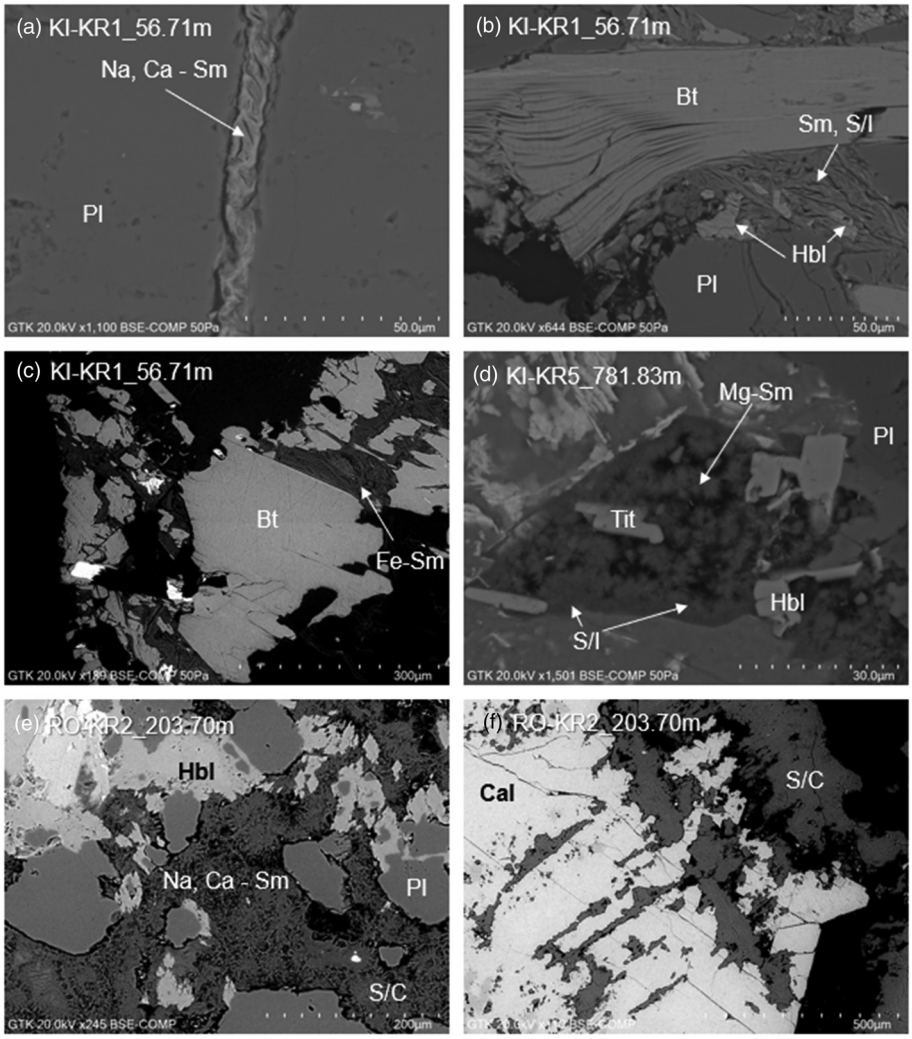

Fig. 6. SEM images of clay fracture filling in polished thin sections. (**a**) and (**b**) Clay mineral fracture filling as alteration products of (**a**) feldspar and (**b**) biotite along the fractures. (**c**) Fe-rich smectite formation as a product of biotite alteration (**d**) complete transformation of amphibole to Mg-smectite in the centre of the grain and to S/I on the rim of the grain. (**e**) Alteration of silicate minerals to clay minerals and (**f**) calcite replacing clay mineral as a product of hydrothermal activity. Abbreviations: Pl, plagioclase; Na,Ca-Sm, Na and Ca bearing smectite; Bt, biotite, Sm, smectite; S/I, smectite-illite; Hbl, hornblende; Fe-Sm, Fe bearing smectite; Mg-Sm, Mg bearing smectite; Tit, titanite; S/C, smectite-chlorite.

hydrothermal alteration has been strongly oxidizing, leading to the thorough hematization of biotite and the alteration of feldspars to clays in the affected zones (Gehör *et al.* 1995).

Fractures with an alteration halo, filled with clays and secondary minerals (calcite, iron sulfide, iron oxide and hydroxides) were found in the studied samples. Hydrothermal phases observed consisted mainly of carbonates and clay minerals (smectite, S/I and S/C). Of these, smectites were detected along both open and closed fractures, although most of the fractures examined in the drill cores were classified as open. XCT was found useful for thin section location

Table 3. Overview on the minerals identified in SEM-EDS analysis performed on cut drill-core samples and thin sections

Sample ID	Sample type	Clay minerals observed including smectites	Main silicates and accessory minerals
KI-KR1_ 56.71	Cut drill core	S/I, S/C, Mg-Sm	Kfs, Bt, Chl, FeOx, Alb
KI-KR1_56.71	Thin section	Na-Sm, S/I, Fe-Sm	Hbl, Rut, Pl, Bt, Kfs
KI-KR1_398.58	Cut drill core	S/C, V/C, Na-Sm	Flu, Syn, Alb,Chl, Amp
KI-KR1_561.95	Cut drill core	Na-Sm, S/I	Pl, Bt, Ms, Amp, Cal
KI-KR1_650.70	Cut drill core	Ca-Sm, Na-Sm, S/C	Amp, Cal
KI-KR5_669.47	Cut drill core	S/I, Na-Sm, Ilt	Bt, Chl, Pl, Kfs
KI-KR5_781.83	Cut drill core	Na-Sm, Sm, S/I, S/C	Amp, Bt, Ms, Kfs, Chl, FeOx, Pl, Apt
KI-KR5_781.83	Thin section	Mg-Sm, Ca-Sm, S/I	Amp, Kfs, Pl, Cal, Tit, Fe silicate, Chl
RO-KR2_203.70	Cut drill core	Na-Sm, S/I	Qz, Bt, Ca-Pl, Kfs, Gth
RO-KR2_203.70	Thin section	Na-Ca_Sm, Mg-Sm (Sap), S/C, S/I	Pl, Kfs, Qz, Amp, Bt
RO-KR2_306.77	Cut drill core	S/I, Ca-Sm, Na-Sm, I/C, S/C	Bt, Ms, Kfs, Pl, Amp, Chl, FeOx
RO_KR2_397.12	Cut drill core	Mg-Sm, Ca-Sm, S/C	Bt, Pl, Hbl, Chl, Cal
RO-KR2_441.57	Cut drill core	Na-Sm	Amp, Ms, Bt, Pl, Chl, Cal
RO-KR2_574.92	Cut drill core	S/C, Na-Sm	Kfs, Bt, Chl
RO-KR2_882.35	Cut drill core	Na-Sm, Ca-Sm, Mg-Sm, S/I	Bt, Pl, Kfs, Phl, Chl

Clay mineral abbreviations: Ca-Sm, Ca-smectite; Fe-Sm, Fe-smectite; I/C, illite–chlorite; Ilt, illite; Mg-Sm, Mg-smectite; Mg-Sm (Sap), Mg-smectite (saponite); Na-Ca_Sm, Na–Ca-smectite; Na-Sm, Na-smectite; S/C, smectite–chlorite; S/I, smectite–illite; Sm, smectite; V/C, vermiculite–chlorite.
Silicates and accessory mineral abbreviations: Kfs, K-feldspar; Bt, biotite; Chl, chlorite; FeOx, iron oxide; Alb, albite; Hbl, hornblende; Rut, rutile; Pl, plagioclase; Flu, fluorite; Syn, synchysite; Amp, Amphibole; Ms, muscovite; Cal, calcite; Apt, apatite; Tit, titanite; Fe silicate, iron silicate; Qz, quartz; Ca-Pl, calcium bearing plagioclase; Gth, goethite. See Supplementary material 3 for all data.

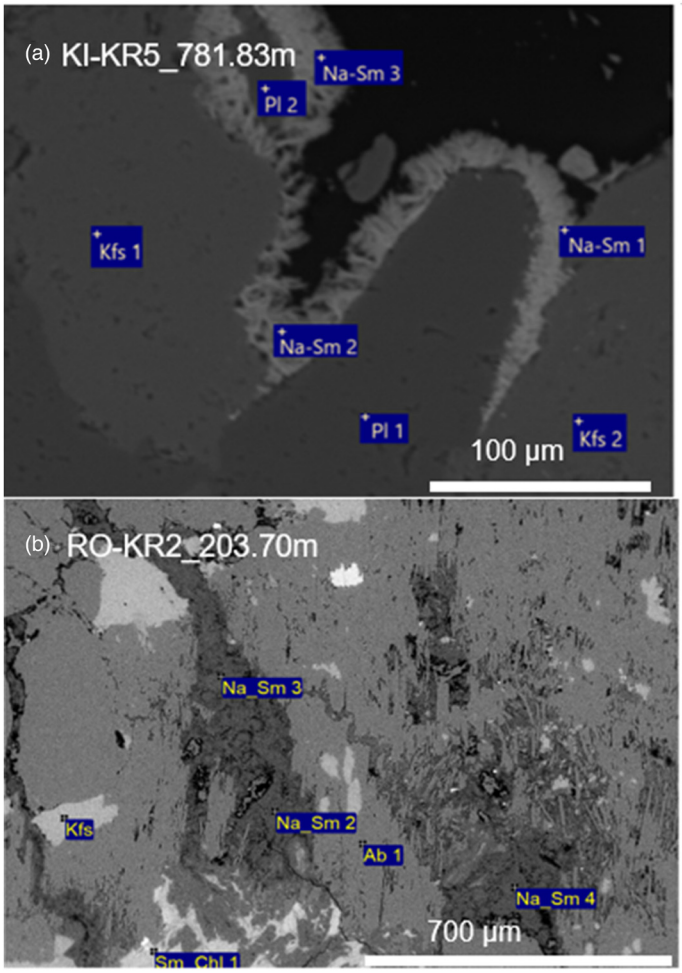

Na-smectite after feldspar dissolution

Spectrum	Na_2O	MgO	Al_2O_3	SiO_2	K_2O	CaO	FeO	Total
Pl 1	9.4		22.6	63.7		4.2		100
Pl 2	8.5		22.4	64.8		4.3		100
Kfs 1	1.2		17.3	68.2	13.4			100
Kfs 2	0.9		18.6	67.7	12.9			100
Na-Sm 1	3.0	4.5	14.4	44.3		3.2	30.6	100
Na-Sm 2	2.8	4.7	14.8	45.9		2.9	28.9	100
Na-Sm 3	3.4	2.5	13.8	44.5		2.3	33.5	100

Na-smectite after feldspar dissolution

Spectrum	Na_2O	MgO	Al_2O_3	SiO_2	K_2O	CaO	FeO	Total
Ab 1	11.6		19.1	69.3				100
Kfs			15.7	71.3	13.0			100
Sm_Chl 1	1.3	16.3	17.9	43.1		1.0	20.5	100
Na_Sm 2	1.0	21.3	20.2	51.0		2.4	4.2	100
Na_Sm 3	1.4	19.9	20.8	51.2		2.6	4.1	100
Na_Sm 4	1.0	20.3	20.0	51.9		2.4	4.4	100

Fig. 7. Examples of feldspar alteration in SEM micrographs with EDXS analysis of the potential Na-smectites (element %): (**a**) alteration at the rims of the plagioclase grains and (**b**) smectite replacing plagioclase. A high iron content in some samples in clay minerals in (a) is related to the association of Fe minerals, which is also seen in the XRD analysis as the co-occurrence of Sm and Chl for the same fracture as in (a).

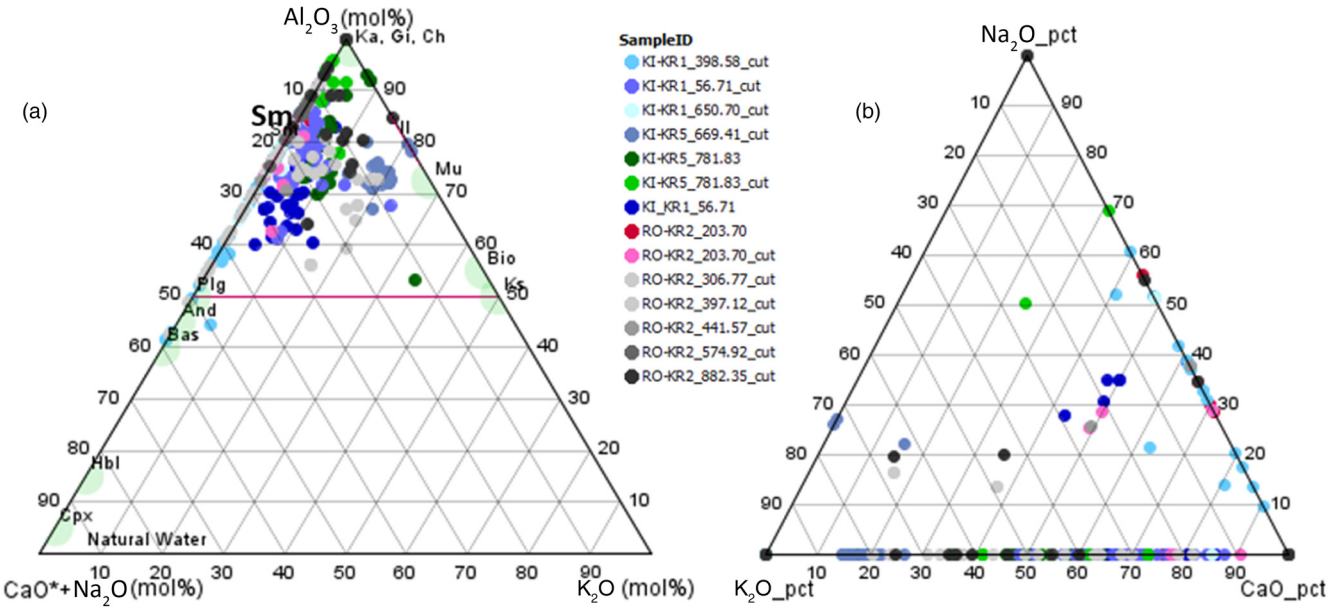

Fig. 8. Scoping geochemical plots of SEM-EDS analyses on clay minerals. (**a**) Overall samples exhibit compositions close to smectites (pale green areas show compositions for minerals indicated in the diagram) and (**b**) the presence of K, Na and Ca in samples show scatter (pct = percentile).
Source: (a) plot based on Nesbitt and Young (1984).

selection. However, thin-section analyses indicate that there are several types of small-scale fractures found in the samples when examined at the microscopic level that are not detectable using XCT.

The most common fracture minerals observed by XRD were calcite and smectite. Smectite occurs in the samples and also commonly as the mixed-layer clays (S/C and S/I) that are found in all samples. Based on the SEM-EDS results, smectites in various compositions can be present in one sample and in the same fractures. This is typical of smectites formed via *in situ* alteration of different minerals, where smectite formation reflects the composition of the parent mineral. SEM-BSE imaging of the fracture filling of cut drill-core samples showed that smectite is the main pure clay mineral, and most of the smectite particles displayed both honeycomb/cellular and cornflake textures, as well as flaky shapes.

Petrographical analyses support the hydrothermal origin of the smectites in the fractures and their *in situ* occurrence as alteration products of the parent minerals. The alteration patterns observed followed the typical patterns (e.g. Fulignati 2020) of hydrolysis reactions at the expense of silicate phases, (plagioclase, feldspar and amphiboles being the most important ones at the sites studied). In the thin sections examined in this study, replacement of parent minerals by clays were observed *in situ* via:

- feldspars or amphibole → Na–Ca-smectite;
- amphiboles and chlorite → Mg-smectite; and
- biotite → chlorite → Fe-smectite.

This suggests that smectite formation occurred during hydrothermal events (acidic or neutral pH of *c*. 5.5–7, low temperatures <160°C: e.g. Fulignati 2020) that are older than the recent groundwater ages (mostly younger than the last glaciation in the area). Co-occurrence of synchysite supports the low-temperature hydrothermal origin of smectite.

Defining the exact smectite mineralogy has uncertainties due to the limitations of the methods used. However, the SEM images in Figures 5–7 and the SEM-EDS analyses (see Supplementary material 3) show considerable compositional differences between the various types of clay minerals in the samples studied, allowing the observation of Na–Ca-smectites, Mg-smectites and Fe-smectites supported by the typical smectite honeycomb and cellular textures in the BSE images. In addition, compositions of S/C and S/I were observed, sometimes displaying a clear alteration pattern from the altered parent mineral, through an interstratified phase to a pure smectite composition. Pure smectites were also observed to be directly replacing minerals without interstratified minerals present. Based on the XRD and SEM examinations, the Na–Ca-smectites were identified as montmorillonite, confirming the presence of bentonite buffer-relevant smectites in bedrock fractures.

Most of the samples obtained were located in fractures that have had recent groundwater circulation (open fractures). As both sites are likely to have had fresh groundwater conditions prior to the latest glaciation and subsequent glacial retreat, meteoric water infiltration has been ongoing for extended periods of time (e.g. Anttila *et al.* 1999*a*, *b*). In Table 2, the known hydrogeological conditions around the sampled core are provided for context with regard to groundwater flow, showing that smectite is (including Na-montmorillonite) observed *in situ,* even in fractures with measured groundwater flow, supporting the stability of smectites. As various types of smectites are possible in bedrock fractures, it is difficult to assess to what extent subsequent alteration of ECC in montmorillonite has taken place. In the samples analysed, Ca-form is more pronounced, complying with the overall understanding from previous studies (Pitkänen *et al.* 1996, 1998).

To assess the natural analogue of fracture-filling clays to bentonite buffer potentially intruding into/in contact with fractures in the host rock in the geological repository conditions, the overall mineralogy needs to be considered. At both sites, mineralogical parageneses are complex and smectites do not occur as monomineralic masses in any of the fracture fillings studied. However, bentonites that may be used as the buffer material in a radioactive waste repository are also known to have accessory minerals, and the differences in the overall mineralogical composition between bentonites in the repository and the fracture-filling materials analysed in the present study are not expected to be unreasonably large. Although no quantitative data are available for the fracture minerals present, a rough comparison can be made between the XRD major and minor/trace phases and bentonite composition. The same minerals can be found in the smectite-bearing fractures as in the bentonites (smectite, muscovite, quartz, plagioclase, K-feldspar, pyrite, calcite and illite) (Fig. 9). The occurrence of abundant chlorite is the most significant difference compared with the reference bentonite buffer overall mineralogy discussed here (Kiviranta *et al.* 2017), although chlorite can be a component in bentonites in general. The natural analogue presented is conceptualized schematically in Figure 9. Similar conceptualization has been used previously as a basis for natural analogues for bentonite stability by, for example, Reijonen *et al.* (2024) for fresh to saline groundwater environments and Reijonen and Alexander (2015) for brine conditions.

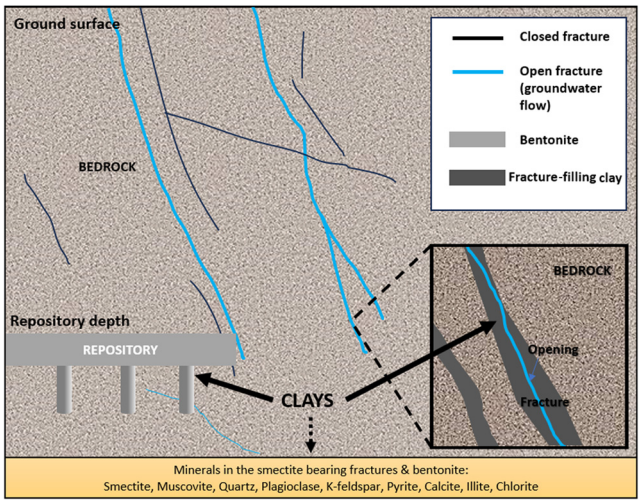

Fig. 9. Conceptual image of fractured crystalline bedrock hosting a repository with bentonite-based backfill and the analogous fracture-filling materials studied here. Mineralogically similar localities are indicated with black arrows.

Conclusions

Hydrothermal microcrystalline clays are found in the fractures of granitic bedrock *in situ* at two sites, Kivetty and Romuvaara, in Finland (ranging to well below repository-relevant depths: i.e. below 500 m). They consist of smectites, illite and chlorite, and associated mixed-layer clays (S/C and S/I), and reflect their parent mineral compositions. They were formed in hydrothermal low-temperature environments (estimates ranging from the Precambrian to at least 250 Myr ago), prior to development of the current groundwater regime. The results presented here further define the alteration mineralogy reported from both sites (Gehör *et al.* 1996*a*, *b*), expanding the clay mineral observations from kaolinite, montmorillonite and smectite clay mineral mixtures towards specific smectite species. The occurrence of Na- and Ca-type smectites/montmorillonites indicates that both compositions may prevail in the current fresh groundwater regimes. Moreover, the *in situ* occurrence of smectite, shown in the petrographical assessment, suggests that no erosion/resedimentation of clays in fractures has occurred since the hydrothermal alteration event.

While no simple montmorillonite locality was observed, smectites are present throughout the system, including Na-bearing smectites (here assigned to be montmorillonites). In open fractures, where groundwater movement is slow – as is to be expected around the deposition hole of a geological radioactive waste repository – results presented here indicate smectite stability in low-salinity groundwater conditions.

Further method development is required to investigate small quantities of smectite occurring in fracture systems to obtain detailed quantitative descriptions of smectite mineralogy and exchanger compositions. One option for obtaining such samples would be direct sampling from, for example, tunnel excavations, which would remove the possibility of potential loss of samples by drilling.

Acknowledgements Heikki Nurmi (Geological Survey of Finland) is thanked for help in the initial sampling campaign at the Loppi drill-core storage facility in Finland. Russell Alexander (Bedrock Geosciences) and Pasi Heikkilä (Geological Survey of Finland) are acknowledged for their useful comments during the writing of this paper. The anonymous reviewers of *Geoenergy* are thanked for their fruitful comments on the manuscript.

Author contributions **HMR**: conceptualization (lead), data curation (equal), formal analysis (equal), funding acquisition (lead), investigation (lead), methodology (equal), project administration (lead), software (lead), visualization (lead), writing – original draft (lead), writing – review & editing (lead); **TA-A**: data curation (equal), formal analysis (equal), investigation (supporting), methodology (supporting), visualization (supporting), writing – original draft (supporting), writing – review & editing (supporting); **TE**: data curation (equal), formal analysis (equal), investigation (supporting), methodology (supporting), writing – original draft (supporting), writing – review & editing (supporting); **JK**: data curation (equal), formal analysis (equal), investigation (supporting), methodology (equal), visualization (supporting), writing – original draft (supporting), writing – review & editing (supporting); **KI**: data curation (supporting), formal analysis (supporting), methodology (supporting), writing – review & editing (supporting); **RL**: conceptualization (supporting), writing – original draft (supporting), writing – review & editing (supporting).

Funding Posiva Oy, Eurajoki, Finland partially funded this research.

Competing interests The authors declare the following financial interests that may be considered as potential competing interests: the work was conducted partially within a company-funded (Posiva Oy) project. No other competing interests are identified.

Data availability One dataset generated during and/or analysed during the current study are available in the Fairdata.fi repository, https://doi.org/10.23729/1ce75faa-d52a-43cd-af40-3961b3081f70. Two other sets of supplementary material (Supplementary material 2 and Supplementary Material 3) generated or analysed during this study are included in this published article (and its supplementary information files). Raw data are available from the corresponding author on reasonable request.

References

Aaltonen, I., Front, K., Gehör, S. and Sahlstedt, E. 2018. *Hydrothermal Alteration of Bedrock at Olkiluoto*. Posiva Report 2018-3.Posiva Oy, Eurajoki, Finland.

Alekseyev, V.A., Medvedeva, L.S., Prisyagina, N.I., Meshalkin, S.S. and Balabin, A.I. 1997. Change in the dissolution rates of alkali feldspars as a result of secondary mineral precipitation and approach to equilibrium. *Geochimica et Cosmochimica Acta*, **61**, 1125–1142, https://doi.org/10.1016/S0016-7037(96)00405-X

Alonso, U., Missana, T., Fernández, A.M. and García-Gutiérrez, M. 2018. Erosion behaviour of raw bentonites under compacted and confined conditions: Relevance of smectite content and clay/water interactions. *Applied Geochemistry*, **94**, 11–20, https://doi.org/10.1016/j.apgeochem.2018.04.012

Alonso, U., Missana, T., García-Gutiérrez, M., Morejón, J., Mingarro, M. and Fernández, A.M. 2019. *CIEMATstudies within POSKBAR Project – Bentonite Expansion, Sedimentation and Erosion in Artificial Fractures*. SKB Technical Report TR-19-08. Svensk Kärnbränslehantering AB (SKB), Solna, Sweden.

Anttila, P., Paulamaki, S., Lindberg, A., Paananen, M., Koistinen, T., Front, K. and Pitkänen, P. 1992. *The Geology of the Kivetty Area, Summary Report*. Report YJT-92-07. Nuclear Waste Commission of Finnish Power Companies, Helsinki.

Anttila, P., Ahokas, H. *et al.* 1999*a*. *Final Disposal of Spent Nuclear Fuel in Finnish Bedrock – Kivetty Site Report*. Posiva Report 99-09. Posiva Oy, Helsinki.

Anttila, P., Ahokas, H. *et al.* 1999*b*. *Final Disposal of Spent Nuclear Fuel in Finnish Bedrock – Romuvaara Site Report*. Posiva Report 99-11. Posiva Oy, Helsinki.

ASC 2023. *Recommendations on Postclosure Aspects of Generic Standards for the Permanent Disposal of Spent Nuclear Fuel and High-Level and Transuranic Radioactive Wastes in the United States*. American Nuclear Society (ASC), Downers Grove, IL.

Baik, M.-H., Cho, W.-J. and Hahn, P.-S. 2007. Erosion of bentonite particles at the interface of a compacted bentonite and a fractured granite. *Engineering Geology*, **91**, 229–239, https://doi.org/10.1016/j.enggeo.2007.02.002

Birgersson, M., Börgesson, L., Hedström, M., Karland, O. and Nilsson, U. 2008. *Bentonite Erosion: Final Report,* SKB Technical Report TR-09-34. Svensk Kärnbränslehantering AB (SKB), Solna, Sweden.

Börgesson, L., Hedström, M., Birgerssonm, M. and Karnland, O. 2018. *Bentonite Swelling into Fractures at Conditions Above the Critical Coagulation Concentration*. SKB Report TR-17-11. Svensk Kärnbränslehantering AB (SKB), Solna, Sweden.

Brindley, G.W. and Brown, G. (eds) 1980. *Crustal Structures of Clay Minerals and Their X-Ray Identification*. Mineral Society Monographs, **5**, https://doi.org/10.1180/mono-5

Claesson Liljedahl, L., Kontula, A. *et al.* 2016. *The Greenland Analogue Project: Final Report*. SKB Technical Report TR-14-13. Svensk Kärnbränslehantering AB (SKB), Solna, Sweden.

Elminen, T., Zwingmann, H. and Kaakinen, A. 2018. Constraining the timing of brittle deformation and sedimentation in southern Finland: Implications for Neoproterozoic evolution of the eastern Fennoscandian shield. *Precambrian Research*, **304**, 110–124, https://doi.org/10.1016/j.precamres.2017.10.014

Eronen, M., Glückert, G., van De Plassche, O., van der Plicht, J. and Rantala, P. 1995. *Land Uplift in the Olkiluoto-Pyhäjärvi Area, Southwestern Finland, During Last 8000 Years*. Report YJT-95-17. Nuclear Waste Commission of Finnish Power Companies, Helsinki.

Fesharaki, O., García-Romero, E., Cuevas-González, J. and López-Martínez, N. 2007. Clay mineral genesis and chemical evolution in the Miocene sediments of Somosaguas, Madrid Basin, Spain. *Clay Minerals*, **42**, 187–201, https://doi.org/10.1180/claymin.2007.042.2.05

Front, K., Paulamäki, S. and Paananen, M. 1998. *Updated Lithological Bedrock Model of the Olkiluoto Study Site, Eurajoki, Southwestern Finland*. Posiva Working Report 98-57. Posiva Oy, Helsinki [in Finnish with an English abstract].

Fulignati, P. 2020. Clay minerals in hydrothermal systems. *Minerals*, **10**, 919, https://doi.org/10.3390/min10100919

Gehör, S. 2007. *Mineralogical Characterization of Gouge Fillings in ONKALO Facility at Olkiluoto*. Posiva Working Report 2007-33. Posiva Oy, Olkiluoto, Finland.

Gehör, S., Karki, A., Suopera, S. and Taikina-aho, O. 1995. *Kivetty, Aanekoski: Petrology of Drill Core Samples and Their Low Temperature Fracture Minerals*. Working Report PATU-95-86. Teollisuuden Voima Oy, Helsinki [in Finnish with an English abstract].

Gehör, S., Karki, A., Maatta, T., Suopera, S. and Taikina-aho, O. 1996*a*. *Kivetty, Aanekoski: Petrology and Low Temperature Fracture Minerals in Drill Core Samples from the Borehole KI-KR10*. Posiva Working Report PATU-96-31. Posiva Oy, Helsinki [in Finnish with English abstract].

Gehör, S., Kärki, A., Suoperä, S. and Taikina-aho, O. 1996*b*. *Kuhmon Romuvaaran Kairausnäytteetm RO-KR10 Petrologia ja Matalan Lämpötilan Rakomineraalit*. Posiva Working Report PATU-96-30. Posiva Oy, Helsinki [in Finnish with English abstract].

Gehör, S., Kärki, A., Suoperä, S. and Taikina-aho, O. 1997*a*. *Kivetty, Äänekoski: Petrology and Low Temperature Minerals in the K1-K11 Drill Core Samples*. Posiva Working Report 1997-16. Posiva Oy, Helsinki, Finland.

Gehör, S., Kärki, A. and Taikina-aho, O. 1997*b*. *Loviisa, Hästholmen: Petrology and Low Temperature Fracture Minerals in Drill Core Samples HH-KR1, HH-KR2 and HH-KR3*. Posiva Working Report 1997-40. Posiva Oy, Helsinki.

Gehor, S., Karki, A., Suopera, S. and Taikina-aho, O. 1998. *Kivetty, Aanekoski: Petrology and Low Temperature Fracture Minerals in the KI-KR12 and KI-KR13 Drill Cores*. Posiva Working Report 98-35. Posiva Oy, Helsinki [in Finnish with an English abstract].

Hall, A.M., Putkinen, N., Hietala, S., Lindsberg, E. and Holma, M. 2021. Ultra-slow cratonic denudation in Finland since 1.5 Ga indicated by tiered unconformities and impact structures. *Precambrian Research*, **352**, 106000, https://doi.org/10.1016/j.precamres.2020.106000

Hedström, M., Ekvy Hansen, E. and Nilsson, U. 2016. *Montmorillonite Phase Behaviour. Relevance for Buffer Erosion in Dilute Groundwater*. SKB Report TR-15-07. Svensk Kärnbränslehantering AB (SKB), Solna, Sweden.

Hedström, M., Nilsson, U. and Lamminmäki, R. 2023. Experimental study of montmorillonite erosion in low ionic strength water under stagnant and flow conditions in artificial fractures. *Applied Clay Science*, **239**, 106929, https://doi.org/10.1016/j.clay.2023.106929

Hjerpe, T., Marcos, N., Ikonen, A.T.K., Reijonen, H. and Åstrand, P.-G. 2021. *Safety Case for the Operating Licence Application: FEP Database Report*. Posiva Working Report 2020-19. Posiva Oy, Eurajoki, Finland.

Iacoviello, F., Giorgetti, G., Nieto, F. and Turbanti Memmi, I. 2012. Evolution with depth from detrital to authigenic smectites in sediments from AND-2A

drill core (McMurdo Sound, Antarctica). *Clay Minerals*, **47**, 481–498, https://doi.org/10.1180/claymin.2012.047.4.07

Kadir, S. 2007. Mineralogy, geochemistry and genesis of smectite in Pliocene volcaniclastic rocks of the Doganbey Formation, Beyşehir basin, Konya, Turkey. *Clays and Clay Minerals*, **55**, 402–422, https://doi.org/10.1346/CCMN.2007.0550408

Kärki, A., Gehör, S., Suoperä, S. and Taikina-aho, O. 1997. *Romuvaara, Kuhmo: Petrology and Low Temperature Fracture Minerals in the R0–R11 Drill Core Samples*. Posiva Working Report 1997-19. Posiva Oy, Helsinki [in Finnish with an English abstract].

Kaufhold, S. and Dohrmann, R. 2008. Detachment of colloidal particles from bentonites in water. *Applied Clay Science*, **39**, 50–59, https://doi.org/10.1016/j.clay.2007.04.008

Kiviranta, L., Kumpulainen, S., Pintado, X., Karttunen, P. and Schatz, T. 2017. *Characterization of Bentonite and Clay Materials 2012–2015*. Posiva Working Report 2016-05. Posiva Oy, Eurajoki, Finland.

Larson, S.Å., Tullborg, E.-L., Cederbom, C. and Stiberg, J.P. 1999. Sveconorwegian and Caledonian foreland basins in the Baltic Shield revealed by fission-track thermochronology. *Terra Nova*, **11**, 210–215, https://doi.org/10.1046/j.1365-3121.1999.00249.x

Lima, M.F., Pamplona, J. and Braga, M.A.S. 2011. Mineralogical and geochemical study of clay and calcite veins in a shear zone related to a sulphur spring (NW Portugal). *Comptes Rendus Geoscience*, **343**, 417–430, https://doi.org/10.1016/j.crte.2011.05.001

Lindberg, A. and Paananen, M. 1989. *Petrography, Lithogeochemistry and Petrophysics of Rock Samples from the Kivetty Study Site, Konginkangas, Central Finland. Part I Drill Hole KI-KRI*. Site Investigations Work Report 89-42.Teollisuuden Voima Oy, Helsinki

Lindberg, A. and Paananen, M. 1990. *Petrography, Lithogeochemistry and Petrophysics of Rock Samples from the Kivetty Study Site, Konginkangas, Central Finland. Part II Drill Holes KI-KR2, KI-KR3, KI-KR4 and KI-KR5*. Site Investigations Work Report 90-34.Teollisuuden Voima Oy, Helsinki [in Finnish with English abstract].

Lindberg, A. and Paananen, M. 1992. *Petrography, Geochemistry and Petrophysics of Rock Samples from Ki Vetty, Konginkangas, and Syyry, Sievi, Cored Bore Holes KI-KR6B and SY-KR6*. Site Investigations Work Report 92-17.Teollisuuden Voima Oy, Helsinki [in Finnish with English abstract].

Liu, L., Moreno, L. and Neretnieks, I. 2009. A dynamic force balance model for colloidal expansion and its DLVO-based application. *Langmuir*, **25**, 679–687, https://doi.org/10.1021/la8026573

Mänttäri, I., Mattila, J., Zwingmann, H. and Todd, A.J. 2007. *Illite K–Ar Dating of Fault Breccia Samples from ONKALO Underground Research Facility, Olkiluoto, Eurajoki, SW Finland*. Posiva Working Report 2007-67 . Posiva Oy, Eurajoki, Finland.

Marcos, N. 1989. *Native Copper as a Natural Analogue for Copper Canisters*. Report YTJ-89-18. Nuclear Waste Commission of Finnish Power Companies, Helsinki.

Melamed, A., Pitkänen, P., Olin, M., Muurinen, A. and Snellman, M. 1992. Interaction of water and compacted sodium-bentonite in simulated nuclear waste disposal conditions. *MRS Online Proceedings Library*, **257**, 557–566, https://doi.org/10.1557/PROC-257-557

Meunier, A. 2005. *Clays*. Springer, Berlin.

Muurinen, A. and Lehokoinen, J. 1999. Porewater chemistry in compacted bentonite. *Engineering Geology*, **54**, 207–214, https://doi.org/10.1016/S0013-7952(99)00075-7

Muurinen, A., Lehikoinen, J., Melamed, A. and Pitkänen, P. 1996. *Chemical Interaction of Fresh and Saline Waters with Compacted Bentonite*. Research Note 1806. Technical Research Centre of Finland (VTT), Espoo, Finland.

Nagra 2021. *The Nagra Research, Development and Demonstration (RD&D) Plan for the Disposal of Radioactive Waste in Switzerland, Technical Report 21-02*. National Cooperative for the Disposal of Radioactive Waste (Nagra), Wettingen, Switzerland.

NEA 2012. *Methods for Safety Assessment of Geological Disposal Facilities for Radioactive Waste*. NEA Report. Nuclear Energy Agency (NEA)/Organisation for Economic Co-operation and Development (OECD), Paris.

Neretnieks, I., Liu, L. and Moreno, L. 2009. *Mechanisms and Models for Bentonite Erosion*. SKB Report TR-09-35. Svensk Kärnbränslehantering AB (SKB), Solna, Sweden.

Neretnieks, I., Moreno, L. and Liu, L. 2017. *Clay Erosion – Impact of Flocculation and Gravitation*. SKB Report TR-16-11. Svensk Kärnbränslehantering AB (SKB), Solna, Sweden.

Nesbitt, H.W. and Young, G.M. 1984. Prediction of some weathering trends of plutonic and volcanic rocks based on thermodynamic and kinetic considerations. *Geochimica et Cosmochimica Acta*, **48**, 1523–1534, https://doi.org/10.1016/0016-7037(84)90408-3

Nordbäck, N., Mattila, J., Zwingmann, H. and Viola, G. 2023. Precambrian fault reactivation revealed by structural and K/Ar geochronological data from the spent nuclear fuel repository in Olkiluoto, southwestern Finland. *Tectonophysics*, **824**, 229208, https://doi.org/10.1016/j.tecto.2022.229208

Pitkänen, P., Snellman, M., Vuorinen, U. and Leino-Forsman, H. 1996. *Geochemical Modelling Study on the Age and Evolution of the Groundwater at Romuvaara Site*. Posiva Report 96-06. Posiva Oy, Helsinki.

Pitkänen, P., Luukkonen, A., Ruotsalainen, P., Leino-Forsman, H. and Vuorinen, U. 1998. *Geochemical Modelling of Groundwater Evolution and Residence Time at the Kivetty Site*. Posiva Report 98-07. Posiva Oy, Helsinki.

Posiva 2021*a*. *Safety Case for the Operating Licence Application - Design Basis (DB)*. Posiva Report 2021-08. Posiva Oy, Eurajoki, Finland.

Posiva 2021*b*. *Safety Case for the Operating Licence Application – Complementary Considerations (CC)*. Posiva Report 2021-02. Posiva Oy, Eurajoki, Finland.

Posiva 2021*c*. *Buffer, Backfill and Closure Evolution*. Posiva Working Report WR 2021-08. Posiva Oy, Eurajoki, Finland.

Posiva 2021*d*. *Safety Case for the Operating Licence Application – Initial State (IS)*. Posiva Report 2021-05. Posiva Oy, Eurajoki, Finland.

Posiva 2021*e*. *Safety Case for the Operating Licence Application – Performance Assessment and Formulation of Scenarios (PAFOS)*. Posiva Report 2021-06. Posiva Oy, Eurajoki, Finland.

Posiva 2022. *Palaeohydrogeochemical Data, Concepts and Interpretation for the Olkiluoto Site*. Posiva Report 2021-13. Posiva Oy, Eurajoki, Finland.

Pusch, R. 2003. *Design, Construction and Performance of the Clay-Based Isolation of the SFR Silo*. SKB Report R-03-30. Svensk Kärnbränslehantering AB (SKB), Solna, Sweden.

Reid, C., Lunn, R., El Mountassir, G. and Tarantino, A. 2015. A mechanism for bentonite buffer erosion in a fracture with a naturally varying aperture. *Mineralogical Magazine*, **79**, 1485–1494, https://doi.org/10.1180/minmag.2015.079.6.23

Reijonen, H.M. and Alexander, W.R. 2015. Bentonite analogue research related to geological disposal of radioactive waste – current status and future outlook. *Swiss Journal of Geosciences*, **108**, 101–110, https://doi.org/10.1007/s00015-015-0185-0

Reijonen, H.M. and Marcos, N. 2016. Chemical erosion of the bentonite buffer: do we observe it in nature? *Geological Society, London, Special Publications*, **443**, 307–317, https://doi.org/10.1144/SP443.13

Reijonen, H.M., Alexander, W.R. and Norris, S. 2023. Resilience in knowledge management – the case of natural analogues in radioactive waste management. *Process Safety and Environmental Protection*, **180**, 205–222, https://doi.org/10.1016/j.psep.2023.10.008

Reijonen, H.M., Elminen, T., Heikkilä, P., Kuva, J. and Jolis, E. 2024. Enhanced identification of fracture smectites and other alteration minerals via short-wave infrared reflectance at two Finnish crystalline sites, Olkiluoto and Hyrkkölä. *Rock Mechanics and Rock Engineering*, https://doi.org/10.1007/s00603-024-03764-2

RWM 2017. *Geological Disposal – Concept Status Report*. NDA Report NDA/RWM/155. Radioactive Waste Management Ltd (RWM), Didcot, UK.

Schatz, T., Kanerva, N., Martikainen, J., Sane, P., Olin, M., Seppälä, A. and Koskinen, K. 2013. *Buffer Erosion in Dilute Groundwater*. Posiva Report 2012-44. Posiva Oy, Eurajoki, Finland.

Schatz, T., Eriksson, R. *et al.* 2016. *BELBaR Deliverable D2.11*. WP2 Partners Final Report on Bentonite Erosion. European Commission, Luxembourg.

SKB 2011. *Long-Term Safety for the Final Repository for Spent Nuclear Fuel at Forsmark - Main Report of the SR-Site Project*. SKB Technical Report TR-11-01. Svensk Kärnbränslehantering AB (SKB), Solna, Sweden.

SKB 2019. *Climate and Climate-Related Issues for the Safety Evaluation SE-SFL*. SKB Technical Report TR-19-04. Svensk Kärnbränslehantering AB (SKB), Solna, Sweden.

Svoboda, J. 2013. The experimental study of bentonite swelling into fissure. *Clay Minerals*, **48**, 383–389, https://doi.org/10.1180/claymin.2013.048.2.16

Uusinoka, R. and Alkio, R. 1976. Clay minerals with expanding lattice in the crystalline bedrock of Finland. *Bulletin of the International Association of Engineering Geology*, **14**, 105–107, https://doi.org/10.1007/BF02634740

Vartiainen, R. 2005. *Teollisuusmineraali- ja rakenuskivitutkimukset Pohjois-Suomessa vuosina 2002–2004*. Report M 10.4/2005/4. Geological Survey of Finland (GTK), Espoo, Finland [in Finnish with English abstract].

Vilks, P. and Miller, N.H. 2010. *Laboratory Bentonite Erosion Experiments in a Synthetic and a Natural Fracture*. NWMO Report TR-2010-16. Nuclear Waste Management Organization, Toronto, Canada.

Viola, G., Mattila, J., Zwingmann, H., Todd, A. and Raven, M. 2011. *Structural and K/Ar Illite Geochronological Constraints on the Brittle Deformational History of the Olkiluoto Region, SW Finland*. Posiva Working Report 2011-37. Posiva Oy, Eurajoki, Finland.

Viola, G., Zwingmann, H., Mattila, J. and Käpyaho, A. 2013. K–Ar illite age constraints on the Proterozoic formation and reactivation history of a brittle fault in Fennoscandia. *Terra Nova*, **25**, 236–244, https://doi.org/10.1111/ter.12031

Weisenberger, T. and Bucher, K. 2011. Mass transfer and porosity evolution during low temperature water–rock interaction in gneisses of the Simano nappe: Arvigo, Val Calanca, Swiss Alps. *Contributions to Mineralogy and Petrology*, **162**, 61–81, https://doi.org/10.1007/s00410-010-0583-2

Welton, J.E. 2003. *SEM Petrology Atlas*. AAPG Methods in Exploration Series, **4**.

Zhu, C. and Lu, P. 2009. Alkali feldspar dissolution and secondary mineral precipitation in batch systems: 3. Saturation states of product minerals and reaction paths. *Geochimica et Cosmochimica Acta*, **73**, 3171–3200, https://doi.org/10.1016/j.gca.2009.03.015